Deuteron elastic scattering at 110 and 120 MeV

A. C. Betker, C. A. Gagliardi, D. R. Semon, R. E. Tribble, H. M. Xu, and A. F. Zaruba
Cyclotron Institute, Texas A&M University, College Station, Texas 77843
(Received 24 March 1993)

Deuteron elastic scattering cross sections have been measured at 110 and 120 MeV on C, ^{58}Ni, and ^{208}Pb. Optical model potentials have been extracted and compared to deuteron global optical model potentials.

PACS number(s): 24.10.Ht, 25.45.De, 27.20.+n, 27.40.+z

We have measured deuteron elastic scattering cross sections at 110 MeV on C and ^{208}Pb, and at 120 MeV on C and ^{58}Ni, with the Texas A&M K500 cyclotron. The motivation for this experiment is that, except for some limited data above 200 MeV [1], there exists no elastic scattering data above 90 MeV. In order to calculate deuteron optical potentials in the energy range accessible by the K500 cyclotron, 110–160 MeV, these elastic scattering cross sections must be measured. The immediate interest in these data is to obtain optical potentials with which the (d,^{2}He) data taken with the proton spectrometer facility [2] can be analyzed. More generally, these data can be used to extend the deuteron global optical potentials [3,4] to this energy region. To do this the addition of analyzing power data would be useful, but a polarized beam is not available to us at this time.

The experimental setup differed for the two energies only in that the energy detector was changed. A detector telescope was mounted on a turntable that was rotated from $-10°$ to $+60°$. The first element in the telescope was a collimator that, along with the mounting position, defined the solid angle. The solid angles for the two data runs at 110 MeV were 0.159 and 0.128 msr, and for the 120 MeV data it was 0.150 msr. After the collimator was a 1 mm thick transmission mount silicon surface barrier detector for a ΔE signal. For the 110 MeV data this was followed by a 5.08 cm thick, 2.54 cm diameter BaF_2 scintillator coupled to a Hammamatsu R1397 photomultiplier tube and base that provided a total energy signal. The energy resolution for this system was about 2 MeV full width at half maximum (FWHM). In order to improve the resolution, this scintillator was replaced by a NaI scintillator 5.08 cm thick by 1.91 cm diameter, backed by an EMI 9902KB phototube. The energy resolution for the 120 MeV data was 0.96 MeV FWHM. This can be seen in the ^{58}Ni spectrum at 10°, shown in Fig. 1, where both the ground state and 1.45 MeV first excited state are clearly resolved. The beam that did not interact with the target went on to a shielded Faraday cup at 0° which was connected to an integrator. A monitor detector, another BaF_2 scintillator, was mounted at $-20°$ for detector angles less than $+25°$, and at $-45°$ for the larger detector angles. The purpose of this detector was to provide a consistency check on the beam current integration and to provide the correct normalization at the smallest angles where the beam intensity was so low that the integrator was unreliable. An overall systematic normalization uncertainty in our measured cross sections of 5% arises from target thickness nonuniformity and beam current integration.

There are two deuteron global optical model potentials currently available. The first, from Daehnick *et al.* [3], covers the mass range A=27–238. Some ^{12}C and ^{24}Mg data are included at 80 and 90 MeV with reduced weights because not much higher mass data exist at these energies. The full energy range covered is thus 11.8–90 MeV. Both relativistic and nonrelativistic forms of the potential were extracted, but this made little difference when the potentials were extrapolated to our data. The relativistic potential, 79DCVF, was used in the analysis below.

The other global potential is from Bojowald *et al.* [4]. This potential covers the mass range from A = 12–208 and the energy range from 52 to 85 MeV. This group took additional data at 58.7 and 85 MeV on several targets, so their data set includes more higher energy work. Only nonrelativistic potentials were extracted.

Both Daehnick and Bojowald optical potentials have the same general form:

$$
\begin{aligned}
V(r) = & -V_R f(r, r_0, a_0) - iW_S f(r, r_I, a_I) \\
& + i4a_I W_D \frac{d}{dr}\left[f(r, r_I, a_I)\right] \\
& + V_{LS}\left(\frac{\hbar}{m_\pi c}\right)^2 (L \cdot S)\left(\frac{1}{r}\right)\frac{d}{dr}\left[f(r, r_{LS}, a_{LS})\right] \\
& + V_{\text{Coulomb}},
\end{aligned}
$$

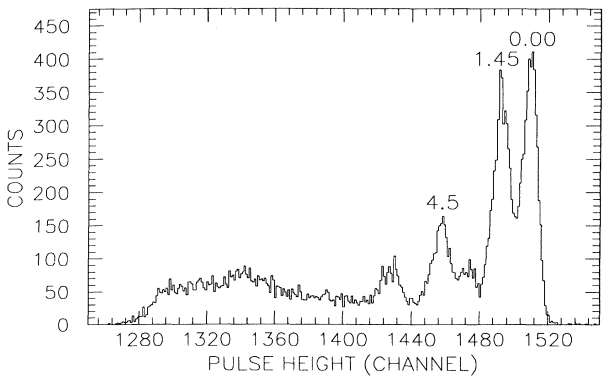

FIG. 1. The 120 MeV ^{58}Ni(d,d)^{58}Ni spectrum at 10°. The resolution of the ground state is 0.96 MeV FWHM. Other states are identified at 1.45 MeV and 4.5 MeV.

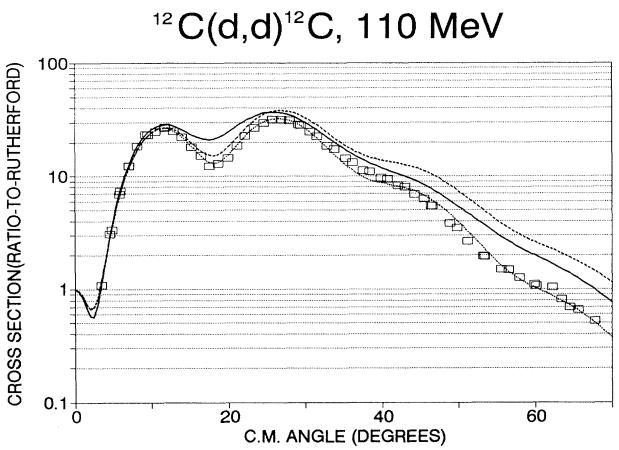

FIG. 2. The 110 MeV carbon data, along with the predictions of two global optical model potentials, and the best fit to the data from these potentials. The solid line is the extrapolation of the Daehnick potential, the dashed line is the extrapolation of the Bojowald potential, and the dotted line is the best fit curve, which in this case used the Bojowald potential as a starting point. In this and the succeeding figures, the statistical errors are much smaller than the data points at the small angles and are comparable to the size of the data points at the largest angles measured.

where

$$f(r, r_i, a_i) = \left[1 + \exp\left(\frac{(r - r_i A^{1/3})}{a_i}\right)\right]^{-1},$$

is the standard Woods-Saxon form.

The higher energy data that are available are from Nguyen Van Sen *et al.* [1]. Cross sections along with vector and tensor analyzing powers were measured on ^{58}Ni from 200 to 700 MeV, and ^{40}Ca at 200 MeV. This group found that the Daehnick potential described the shape of their data well, and provided a good starting point for a fit.

Our carbon data, along with the predictions of the

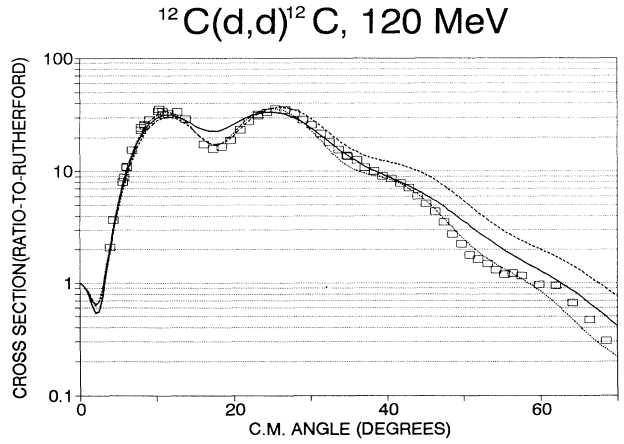

FIG. 3. The 120 MeV carbon data, potentials, and fits, as in Fig. 2. The best fit curve here used the Daehnick 110 MeV best fit curve as a starting point.

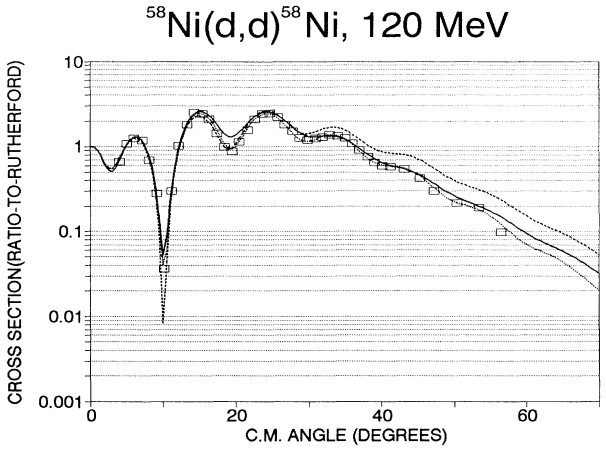

FIG. 4. The 120 MeV ^{58}Ni data, potentials, and fits, as in Fig. 2. The best fit curve used the Daehnick potential as a starting point.

global optical potentials and our best fits, are shown in Figs. 2 and 3. The data vary smoothly from the lower energy data and, as expected, are slightly smaller in cross section and slightly more forward peaked. Note that the Daehnick potential is even more forward peaked than the data at 110 MeV, and the predicted cross section is also larger than the data at scattering angles beyond the first diffraction maximum. At 120 MeV the magnitude of the cross section is about right, suggesting that the calculated cross section of this global model falls faster with energy than the data in this energy range and at this mass. The Bojowald potential has the correct phase, but is too large outside the second diffraction maximum at both energies. Neither of the global models has sufficient diffraction to agree with the data. The fits, carried out with the optical model search code CUPID [5], using the two global potentials as starting points, describe the 110 MeV data well. The fitting was done by chi-square minimization. The 120 MeV data were fit both with the extrapolated potentials and with the potentials that re-

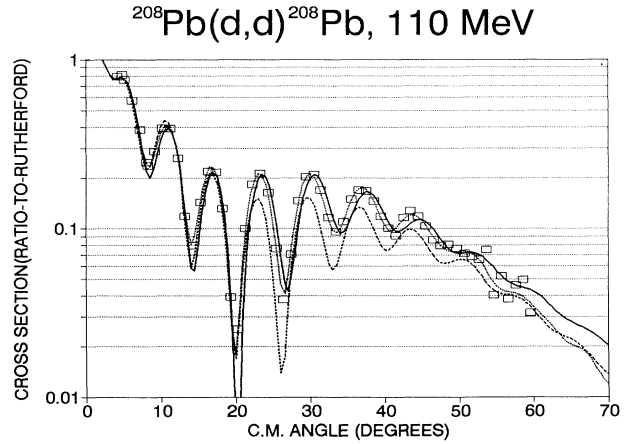

FIG. 5. The 110 MeV ^{208}Pb data, potentials, and fits, as in Fig. 2. The best fit curve used the Daehnick potential as a starting point.

TABLE I. Optical model parameters. The asterisks indicate the best fit parameters for each target and energy.

	V_R	r_0	a_0	W_S	W_D	r_I	a_I	V_{LS}	r_{LS}	a_{LS}	Volume integrals (J/A) Real	Imag.	$L \cdot S$
110 MeV C													
Daehnick	59.18	1.17	0.85	10.82	4.60	1.27	0.67	3.68	1.07	0.66	794	268	19.0
D fit	60.00	1.16	0.77	11.34	4.75	1.32	0.70	3.70	1.12	0.74	721	315	20.0
Bojowald	58.67	1.18	0.72	8.58	4.07	1.27	0.82	6.00	0.87	0.87	685	279	26.0
B fit*	60.17	1.14	0.75	9.12	8.68	1.36	0.74	5.44	0.92	0.90	682	303	25.0
120 MeV C													
Daehnick	56.35	1.17	0.86	12.00	3.72	1.27	0.67	3.36	1.07	0.66	767	256	17.4
D fit	58.30	1.19	0.79	10.72	3.81	1.35	0.71	3.08	1.02	0.75	762	293	15.3
D110 fit*	55.48	1.16	0.78	6.99	3.85	1.33	0.79	4.14	1.42	0.83	672	260	28.4
Bojowald	56.27	1.18	0.72	9.90	3.13	1.27	0.82	6.00	0.87	0.87	657	265	26.0
B fit	54.24	1.15	0.75	10.60	3.15	1.26	0.84	5.99	0.86	0.81	622	281	25.6
B110 fit	60.20	1.15	0.80	8.14	4.18	1.37	0.76	5.61	0.87	0.84	740	296	24.1
120 MeV ^{58}Ni													
Daehnick	60.41	1.17	0.86	12.00	3.72	1.27	0.78	3.36	1.07	0.66	550	192	6.0
D fit*	59.11	1.14	0.84	12.24	3.42	1.28	0.82	6.36	1.18	0.89	501	203	12.6
Bojowald	62.66	1.18	0.77	9.90	4.78	1.27	0.85	6.00	0.93	0.93	553	203	9.4
B fit	59.99	1.15	0.75	9.87	4.60	1.24	0.89	6.16	1.04	1.22	494	197	10.9
110 MeV ^{208}Pb													
Daehnick	69.05	1.17	0.85	10.82	4.60	1.27	0.90	3.68	1.07	0.66	532	165	2.8
D fit*	68.37	1.18	0.81	10.94	4.65	1.29	0.87	5.24	1.11	1.30	538	172	4.2
Bojowald	74.71	1.18	0.84	8.58	7.85	1.27	0.89	6.00	1.01	1.01	588	184	4.3
B fit	68.17	1.19	0.81	8.14	7.33	1.27	0.85	6.54	1.06	1.14	545	168	5.0

sulted from the fits to the 110 MeV data. Both fits that we obtained starting from the extrapolated global potentials were qualitatively poor. The best fit shown in Fig. 3 is the result of using the fit to our 110 MeV data as the starting point. In all cases the diffraction peaks are sensitive to whether or not the spin-orbit term is allowed to vary.

The 120 MeV ^{58}Ni data are shown in Fig. 4, along with the associated potentials and fits. The extrapolation of the Daehnick potential works quite well in this case. The fit starting from the Daehnick parameters only improves the agreement a small amount at the diffraction minima. The Bojowald potential, on the other hand, again does not have enough large angle absorption to fit the data, although this discrepancy is smaller than it is for the carbon target.

Figure 5 shows our 110 MeV ^{208}Pb data. The cross section predicted by the Daehnick potential is again slightly out of phase with the data, this time with the potential less forward peaked, while the predicted magnitude agrees quite well. The Bojowald potential is too low in magnitude at large angles, but has the correct phase. Again, both starting points provide fits that agree with the data quite well.

Table I shows the optical model parameters from the extrapolated global potentials and the fits on all targets and energies. In general, the results of the fits were stable against modest changes in the starting parameters. Both global potentials were qualitatively close. From this limited data set, only a few significant mass and energy dependent patterns can be seen. The Daehnick potential has too large an a_r across the mass range at this energy. It also seems to have an energy dependent absorption that does not agree with the $A = 12$ data. Since the potential was derived for $A = 27$–238, this is an extrapolation that cannot be expected to work well in any case. The absorption on A=58 and 208 agrees very well with the data. The Bojowald potential, on the other hand, has a systematic variation of the absorption as a function of mass at these energies. It is much too small at A=12, too small at A=58, and too large at A=208. With the data available, both potentials provide comparable starting points for optical model fits.

The optical model parameters extracted here can only be considered to be suggestive of those that would result from a global optical potential in this region. Furthermore, the addition of analyzing power data from $(\vec{d}, d)$ scattering would be quite useful in better specifying the potential. This is especially true for the spin-orbit terms. For mass 12, both the phases and the amplitudes of the calculated cross sections were sensitive to whether or not the spin-orbit terms were allowed to vary in our fits. For the heavier nuclei, allowing the spin-orbit terms to vary only improved our fits at the largest angles. Without additional data, more precise parameters cannot be extracted.

This work was supported in part by the U.S. Department of Energy under Grant Nos. DE-FG05-86ER40256 and DE-FG03-93ER40773 and by the Robert A. Welch Foundation.

[1] Nguyen Van Sen *et al.*, Phys. Lett. **156B**, 185 (1985).
[2] A. C. Betker, C. A. Gagliardi, H. M. Xu, and A. F. Zaruba (in preparation); A. C. Betker and C. A. Gagliardi, Nucl. Instrum. Methods **A283**, 67 (1989).
[3] W. W. Daehnick, J. D. Childs, and Z. Vrcelj, Phys. Rev. C **21**, 2253 (1980).
[4] J. Bojowald, H. Machner, H. Nann, W. Orlert, M. Rogge, and P. Turek, Phys. Rev. C **38**, 1153 (1988).
[5] J. R. Comfort, Comput. Phys. Commun. **16**, 35 (1978).